Les Cahiers du GERAD ISSN: 0711–2440

Stochastic orebody modelling and stochastic long-term production scheduling for an iron ore deposit

M.N. Vallejo
R. Dimitrakopoulos

G–2017–93

November 2017

La publication de ces rapports de recherche est rendue possible grâce au soutien de HEC Montréal, Polytechnique Montréal, Université McGill, Université du Québec à Montréal, ainsi que du Fonds de recherche du Québec – Nature et technologies.

Dépôt légal – Bibliothèque et Archives nationales du Québec, 2017
– Bibliothèque et Archives Canada, 2017

The publication of these research reports is made possible thanks to the support of HEC Montréal, Polytechnique Montréal, McGill University, Université du Québec à Montréal, as well as the Fonds de recherche du Québec – Nature et technologies.

Legal deposit – Bibliothèque et Archives nationales du Québec, 2017
– Library and Archives Canada, 2017

GERAD HEC Montréal
3000, chemin de la Côte-Sainte-Catherine
Montréal (Québec) Canada H3T 2A7

Tél. : 514 340-6053
Téléc. : 514 340-5665
info@gerad.ca
www.gerad.ca

Stochastic orebody modelling and stochastic long-term production scheduling for an iron ore deposit

Maria Natalia Vallejo [a]

Roussos Dimitrakopoulos [a,b]

[a] *COSMO – Stochastic Mine Planning Laboratory, Montréal (Québec) Canada, H3A 0E8*

[b] *GERAD & Department of Mining and Materials Engineering, McGill University, FDA Building, Montréal (Québec) Canada, H3A 0E8*

maria.vallejo@mail.mcgill.ca
roussos.dimitrakopoulos@mcgill.ca

November 2017
Les Cahiers du GERAD
G–2017–93

Abstract: For over a decade, stochastic optimization has emerged as a framework that is capable of generating a life-of-mine production schedule that increases net present value, while simultaneously reduces the risk associated with geological uncertainty. This paper focuses on the application of the stochastic strategic mine planning for technical risk management in a real-world iron ore deposit in Quebec, Canada, demonstrating the key steps of the framework. The related approach, firstly, quantifies both the volumetric and multi-element grade uncertainty of the deposit by generating a set of equally-probable scenarios of the orebody. In the case study presented, the boundaries of the iron ore deposit are generated using the pattern-based wavelet simulation algorithm, while the pertinent geological properties, namely, head iron, Davis Tube weight recovery, Davis Tube concentrate iron, and silica content are jointly simulated using the direct block minimum/maximum autocorrelation factor algorithm. Subsequently, the simulated scenarios of the iron deposit serve as input to a life-of-mine stochastic integer programming production scheduling model. The latter optimization model is employed to minimize and manage the risk associated with the geological uncertainty of the deposit, in terms of meeting production targets, while generating an optimal mining sequence of extraction maximizing net present value. The results of the case study serve as valuable input for the conceptual stage of the specific mining project and, in particular, quantify the risk associated with the product's silica content, the total iron production and the expected annual cash flows.

Keywords: Stochastic mine planning, technical risk management, stochastic simulation, open pit mine scheduling, strategic planning

Acknowledgments: This work was funded by the Natural Sciences and Engineering Research Council of Canada (NSERC) Discovery Grant 239019, and Fonds de recherche du Québec-Nature et technologies, FQRNT Grant "Développement d'une stratégie globale d'optimisation de sites miniers avec incertitude: Amélioration de la viabilité économique et de la gestion environnementale des résidus miniers d'une mine de fer dans le nord" with industry collaborator being New Millennium Ltd.

1 Introduction

In general, an optimal open pit mine production schedule is defined as the sequence of extraction that maximizes the present value of a mining project, subject to various technical and operational constraints. Defining a long-term production schedule is one of the most important tasks in the mine planning process because it defines the ore supply over the life-of-mine and, consequently, has a substantial impact on the project's net present value (NPV). Mine production scheduling optimization is a complex process due to its size and the uncertainty of key input models, particularly the supply and quality of ore materials and the demand for the final products sold.

Over the past decade, there have been substantial efforts in developing new models that incorporate geological uncertainty into the mine planning process. One approach is based on stochastic integer programming or SIP (Birge and Louveaux, 2011). SIP models were first introduced and then developed in the context of mining planning by Ramazan and Dimitrakopoulos (2004; 2005; 2013). The model directly maximizes the NPV and manages risk by minimizing deviations from ore, metal and mine production targets by penalizing the scenario-wise deviations (e.g., tonnage surplus or shortage) in the objective function, as well as discounting penalties over production time with the so-termed geological risk discounting (Dimitrakopoulos and Ramazan, 2004). Several examples, extensions and applications follow; for example, Leite (2007) and Leite and Dimitrakopoulos (2014) solve the SIP schedule for a copper mine to obtain a schedule with a 29% higher NPV over the conventional method. Abor and Dimitrakopoulos (2010) show stochastic pushback design and schedules leading to larger final pits than conventional approaches. Benndorf (2005) and Benndorf and Dimitrakopoulos (2013) extend the SIP model to account for several elements of an iron-ore operation, showing that the capability of the stochastic approach to controlling risks of deviating from production targets and product quality constraints. Dimitrakopoulos and Jewbali (2013) use the concept of simulated grade control data to improve stochastic long-term scheduling in a gold mine and significant improvements. Spleit (2014) applies an SIP in a multi-element iron ore mine, and demonstrates that the expected production tonnages and qualities obtained using a conventional orebody model varies significantly when the sensitivity of the design is tested with a set of simulations. The risk-based schedule yields a 5.8% higher NPV than the sequence obtained by the deterministic schedule, with significantly less risk.

These SIP models for optimizing production scheduling are often too large to be solved with conventional solvers. To alleviate this, solution approaches based on (meta-) heuristics to provide high-quality solutions in a reasonable amount of time. Leite (2007) uses a sliding time window. Lamghari and Dimitrakopoulos (2012) propose a metaheuristic method based on Tabu Search (TS) that solves SIP models within a few minutes up to a few hours, compared to commercial solvers that may take days to solve for some applications, if any solution is attainable. Lamghari et al. (2013) propose a more computationally efficient metaheuristic solver using Variable Neighborhood Decent (VND). More recently, metaheuristic algorithms based on simulated annealing have been use to optimize not only singe mining operations but simultaneously groups of mines and related processing streams from mines to products with complex, non-linear processing stream options (Montiel *et al.*, 2016; Goodfellow and Dimtrakopoulos, 2016). Finally, Rimélé (2016) proposes a heuristic that uses the linear relaxation of a simplified model to obtain a fractional schedule, which is then used as a heuristic called Topological Sorting Algorithm (TSA). The methodology is applied to an iron ore mine, and obtains a solution with a 2% optimality gap in 12 minutes, compared to 22 hours using a commercial solver.

Traditionally, orebody resource estimation ignores the presence of geological uncertainty and global as well as local grade variability, resulting in models that smooth-out low- and high-grade variability, while misrepresent the proportions of both lower and higher grade materials in the deposit (e.g. Godoy, 2002). Using these models as inputs to the mine planning process results in unrealistic mine production and financial forecasts, and can have substantial adverse impacts on the real-world performance of the asset. Alternatively, modern Monte Carlo geostatistical or stochastic simulation techniques (Goovaerts, 1997) can be used to create a set of equally-probable representations of the orebody under study that respect grade variability and proportions locally and globally, while as a group, can be used to model and quantify spatial geological uncertainty. Modern simulation methods can deal with spatial complexity, such as curvilinear features of mineral deposit geology and are based on the so-termed multiple-point statistics, including methods such as *SNESIM* (Strebelle, 2002) and *FILTERSIM* (Zhang *et al.,* 2006), and others, mostly focusing on the simula-

tion of categorical variables such as the boundaries of geological units and wireframes of mineralized zones. A more recent and computationally efficient method used in the present study to simulate geological boundaries is *WAVESIM* (Chatterjee *et al.*, 2012), a pattern-based approach shown to perform better than the previously mentioned methods, and it is based on multi-scale decomposition to reduce the size of the geological pattern database and accelerate the pattern searching during the sequential simulation process. The simulation of multiple correlated properties of interest of mineral deposits within simulated geological domains, simulated with methods such as *WAVESIM,* are based on the spatial de-correlation of related elements to orthogonal factors that can be simulated independently. The approach used herein is a combination variable decorrelation based on the so-called Maximum/Minimum Autocorrelation Factors or *MAF* (Desbarats and Dimitrakopoulos, 2000), combined with the direct block simulation method (*DBSIM*) of Godoy (2002), to generate a computationally very efficient approach (*DBMAFSIM*) detailed in Boucher and Dimitrakopoulos (2009). The approach is shown to work well in reproducing the statistical, spatial continuity and cross continuity of multiple correlated variables several studies (e.g. Lopez et al., 2011; Goodfellow et al., 2012).

In the following sections, the general methodology utilized in this study for strategic mine planning, integrating geological uncertainty and managing related risk, is first presented; it includes the stochastic simulation of multi-element mineral deposits, followed by the related stochastic integer programming formulation for life-of-mine production scheduling. Then, an application of the methodology at an iron ore deposit in northern Quebec, Canada, is detailed. Conclusions follow.

2 Methodology for strategic mine planning under uncertainty

This section outlines first the stochastic simulation methods used in the case study, for the simulation of a mineral deposit's geological units and wireframes, and grades or other pertinent attributes of interest to mine planning. Then, a stochastic integer programming formulation for long-term open-pit mine production scheduling optimization, based on the simulated scenarios from the previous step, is presented.

2.1 Stochastic simulation of a multi-element mineral deposit

2.1.1 Simulation of geological units and wireframes

The simulations of categorical variables, such as rock types and lithologies, can be modelled using MP or pattern-based simulation methods. This section is dedicated to outlining the steps for categorical simulation using wavelet decomposition, *WAVESIM.* For more details, the reader is referred to (Chatterjee et al., 2012). The key steps of the *WAVESIM* algorithm are as follows*:*

1. Create a pattern database by scanning the training image.
2. Decompose the patterns using wavelet analysis.
3. Group the patterns into classes using the k-means clustering algorithm.
4. Calculate the prototypes that represent the k-classes of patterns.
5. Define random path visiting all nodes to be simulated.
6. For each node to be simulated:
    i. Find the neighborhood of conditioning data, which defines a data event.
    ii. Compare data event to prototypes and select the most similar prototype class.
    iii. Using the patterns within the selected class, create a conditional probability density function (*cpdf*) for the category of the central node of the pattern. Randomly select a category for the central node.
    iv. Randomly choose a pattern from the subset within the class that have the previously selected central-node category.
7. Repeat steps 5 and 6 to generate multiple realizations.

Generating the pattern database

The first step to perform orebody simulation using *WAVESIM* is to generate of the pattern database. The TI is "scanned" using a template, T. A pattern is obtained by centering T on each of the nodes in the TI as is shown in Figure 1(a). Afterwards, the obtained patterns are stored as a set of vectors in the form of a pattern database, Figure 1(b).

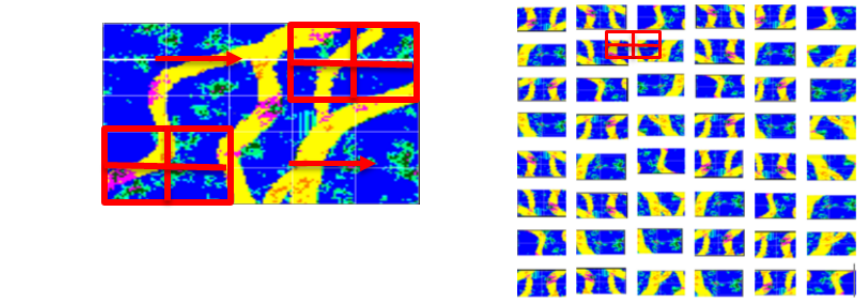

a) Training Image and Template (red rectangle) b) Pattern database

Figure 1: Generation of a pattern database.

Dimensional reduction of the pattern database and classification

After generating the pattern database, the patterns are divided into classes to allow a faster simulation process. To classify the patterns, *WAVESIM* obtains a wavelet-based representation of the patterns through wavelet decomposition. This algorithm aims to provide an approximate sub-image of the patterns for data compression purposes. From the wavelet decomposition, the information of the approximate sub-band of the nearby pixels that describe a pattern is obtained. The approximate sub-band of an image is considered to be a sufficient representation of the complete image. After reducing dimensionality, patterns are classified using the approximated sub-bands of the patterns. *WAVESIM* separates the patterns into k classes ("clusters") using k-means clustering technique (Ding and He, 2004).

Pattern-based simulation

After the pattern database is compressed and classified, the prototypes of the classes are calculated. The prototypes are obtained by a pixel-wise averaging of all patterns that belong to each class. These prototypes are used during the simulation process when the similarity measure between the conditional data event and the patterns is calculated. The similarity metric is only calculated between the data event and the prototypes of each class, where similarity is measured using the L2-norm of the pixel-wise distance between the prototypes and the conditioning data. Subsequently, the class with the lowest distance (highest similarity) is chosen. For categorical simulation, a *cpdf* is built for each of the values of the central node within the prototype's class. A Monte-Carlo sampling is done over this *cpdf* to choose the category of the central node. Following this, a pattern is randomly selected from the subset of patterns within the prototype class that have the central nodes belonging to the same category drawn in the previous Monte-Carlo sampling. The selected pattern is pasted onto the simulation grid. Here, a parameter defines whether the innermost portion (inner patch) of the pattern is stored. This set of innermost nodes will not be revisited during the simulation, and only the nodes outside this inner-patch will be re-simulated.

2.1.2 Joint block simulation of multiple geological attributes of interest

This section outlines the steps to generate simulations of continuous correlated variables directly at the block support. For further details pertaining the direct block simulation method based on minimum/maximum autocorrelation factors (MAF) or *DBMAFSIM* the reader is referred to (Boucher and Dimitrakopoulos, 2012). The simulation algorithm proceeds as follows:

1. Transform multivariate data $Z(u)$ to normal scores $Y(u)$.
2. Transform the normal scores $Y(u)$ to MAF factors $M(u)$.
3. Define a random path to visiting each block.
4. For each block to be simulated:
   i. For each MAF factor, simulate the N points independently using the LU decomposition method (Davis, 1987).
   ii. For each MAF factor, average the group of points to obtain the block support values in the MAF space. The simulated block values are saved as conditioning data for future points.
   iii. For each MAF factor, back-transform the N simulated point values from the MAF-space to the normal score space, $M(u) \rightarrow Y(u)$.
   iv. For each normal score variable, back-transform the values to the original data space, $Y(u) \rightarrow Z(u)$.
5. Repeat steps 3 and 4 to obtain multiple simulations.

Orthogonalization with minimum/maximum autocorrelation factors

MAF performs a linear transformation of a multivariate vector to a new set of variables, called "factors" of the original vector. Consider the stationary vector of K random functions (RFs) $\mathbf{Z}(u) = \left\{Z^1(u), \ldots, Z^k(u)\right\}$, which is transformed to its Gaussian equivalent, $\mathbf{Y}(u) = \left\{\phi_1(Z^1(u)), \ldots, \phi_k(Z^k(u))\right\}$. The resulting vector RF, $Y(u)$, is composed of K Gaussian RFs assumed to be multi-Gaussian. The MAF of the variables are defined as a new vector RF $M(u) = \left\{M^1(u), \ldots, M^k(u)\right\}$, where the K RFs are independent and obtained from the multi-Gaussian vector RF $Y(u)$ using the co-efficient matrix A such that:

$$M(u) = A^T Y(u) \tag{1}$$

where the MAF variables, $M(u)$, are linear functions of $Y(u)$. The derivation of A is equivalent to performing two successive PCA decompositions (Desbarats and Dimitrakopoulos, 2000).

Jointly simulating variables directly at block support

After the variables are decorrelated into MAF space, the factors are simulated independently. *DBMAFSIM* discretizes a block into a set of points, and uses the Lower/Upper (LU) decomposition method (Davis, 1987) to simulate the block's points, conditioned to existing drillholes or previously-simulated points within a search neighborhood. The simulated point values in MAF space are averaged at block-support scale, and serve as conditioning data when simulating future points in the MAF space. The simulated point values, however, are transformed back to the data space. The final simulated block value in the original data space is obtained as follows:

$$z_s^k = \frac{1}{N} \sum_N (\phi^{-1}(A^{-T} m_s^k)) \tag{2}$$

where A is the matrix of MAF coefficients.

2.2 A stochastic integer programing formulation for long-term open-pit mine production scheduling optimization

This stochastic optimization formulation presented in this section been adapted from Rimélé (2016), which is originally based on the SIP proposed by Ramazan and Dimitrakopoulos (2005; 2013). The following notation explained and the formulation follows.

2.2.1 Notation

Sets and indices

$B = \{i = 1, \ldots, N\}$	Set of blocks in the orebody,
$P = \{p = 1, \ldots, P\}$	Set of considered periods for the schedule,
$D = \{d = 1, \ldots, D\}$	Set of destinations available for the blocks,
$S = \{s = 1, \ldots, S\}$	Set of equiprobable orebody simulations,
$\mathcal{C} = C_1 \cup C_2$	Set of block's characteristics,
$\mathcal{C}_1 = \{C_1 = 1, \ldots, C_1\}$	Linear metallurgical characteristics (e.g. tonnages),
$\mathcal{C}_2 = \{C_2 = 1, \ldots, C_2\}$	Non-linear characteristics (grades),
$G(B, A)$	Oriented graph representing the precedence relationships between blocks, $(a, b) \in A$ if $a \in B$ is a predecessor of $b \in B$.
$\mathcal{N}(i)$	Set of neighbours of block i, typically blocks at the North, East, South and West on the same level and one block below.
$\mathcal{B}^{1/2} \subset B$	subset of blocks that form a "checkerboard" pattern in the X, Y and Z directions, i.e., every other block on the 3D grid. This subset is used to ensure that the extraction sequence is mineable.

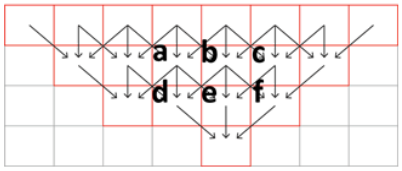

Figure 2: Precedence relationships between blocks (Rimélé, 2016).

$\Gamma_i^+ = \{b \in B; (i, b) \in A\}$	Set of direct successors of block i.
$\Gamma_b^+ = \{d, e, f\}$; . In Fig. 2, $\bar{}_e = \{a, b, c\}$	
Γ_i^{-Tot}	Set of all the predecessors of block i. In Fig. 2, $\Gamma_e^{-Tot} = \{a, b, c\} \cup \bar{}_a^{Tot} \cup \bar{}_b^{Tot} \cup \bar{}_c^{Tot}$

Parameters

$v_{i,d,s}$ Economic value of block i in scenario s if it is sent to destination d. This economic value depends on several parameters:

$$v_{i,d,s} = \begin{cases} -\,E^{cost}_{waste} * t_{i,s} - TH^{cost} * TH_{i,d} & \text{if d} = 0 \Leftrightarrow \text{waste dump} \\ R_{i,s} - P^{cost}_{conc} * conc_{i,s} - E^{cost}_{ore} * t_{i,s} - TH^{cost} * TH_{i,d} & \text{if d} = 1 \Leftrightarrow \text{mill} \end{cases}$$

where:

$R_{i,s}$	Revenue from selling the metal content of block i in scenario s;
$conc_{i,s}$	Concentrate tonnes of block i in scenario s, $conc_{i,s} \in \mathcal{C}_1$;

$$conc_{i,s} = t_{i,s} * Rec_{i,s}$$

$Rec_{i,s}$	Weight recovery of block i in scenario s, obtained from the simulation of the Davis Tube Weight Recovery (used in the case study);
P^{cost}_{conc}	Processing cost of concentrate material per tonne;
E^{cost}_{ore}	Extraction cost of ore material per tonne;
E^{cost}_{waste}	Extraction cost of waste material per tonne;
$TH_{i,d}$	Truck hours needed to send block i to destination d;
TH^{cost}	Cost per truck hour;
$t_{i,s}$	Tonnage of block i in scenario s;
$q_{c_1,i,s}$	Quantity of characteristic c_1 of block i in scenario s;
$g_{c_2,i,s}$	Grade c_2 of block i in scenario s;
$target^{\pm}_{c,p}$	Minimum (-) and maximum (+) targets of quantity or grade c in period p;
$pen^{dev\pm}_{c,\,p}$	Penalty cost of deviation from the targets of quantity or grade c in period p (excess +, shortage -);
r	Discount rate taking into accounts the time value of money and the uncertainty of the future streams of cash flows;
$d_p = \frac{1}{(1+r)^{p-1}}$	Discount factor

Variables

Binary variables:

$$x_{i,d,p} = \begin{cases} 1 & \text{if block i} \in B \text{ is sent to destination } d \in D \text{ by period } p \in P \\ 0 & \text{Otherwise} \end{cases}$$

To simplify the notation, $x_{i,d,p=0} = 0, \forall i \in B, \forall d \in D$. Note that the binary value of the variable is defined by period $p \in P$. This means that $x_{i,d,p} = 1$ if it is mined in or before period p, otherwise $x_{i,d,p} = 0$.

Continuous variables:

$dev^{\pm}_{c,p,s} \in \mathbb{R}^+$ Deviation from the targets in terms of characteristics c for scenario $s \in S$, during period $p \in P$ (excess +, shortage -).

2.2.2 A stochastic integer programing formulation for open-pit mine production scheduling

This section describes the general stochastic open-pit mine production scheduling (SOPMPS) optimization formulation based on stochastic integer programing used in this study.

Objective function

$$\max Z = \overbrace{\frac{1}{S}\sum_{i\in\mathcal{B}}\sum_{d\in\mathcal{D}}\sum_{p\in\mathcal{P}}\sum_{s\in\mathcal{S}} d_p \cdot v_{i,d,s} \cdot (x_{i,d,p} - x_{i,d,p-1})}^{\text{Part 1}} - \overbrace{\frac{1}{S}\sum_{c\in\mathcal{C}}\sum_{p\in\mathcal{P}}\sum_{s\in\mathcal{S}} d_p \cdot \left(pen^{dev+}_{c,p} \cdot dev^{+}_{c,p,\ s} + pen^{dev-}_{c,p} \cdot dev^{-}_{c,p,s}\right)}^{\text{Part 2}} \quad (3)$$

The objective function is comprised of two parts. *Part* 1 aims to maximize the expected net present value, while *Part* 2 minimizes the expected costs associated with deviating from the production targets. Specifically, this part is used to minimize the risk that arises from geological uncertainty.

Constraints

Reserve constraints

$$x_{i,d,p} - x_{i,d,p-1} \geq 0 \qquad \forall i \in \mathcal{B},\ \forall d \in \mathcal{D},\ \forall p \in \mathcal{P} \quad (4)$$

$$\sum_{d\in\mathcal{D}} x_{i,d,p} \leq 1 \qquad \forall i \in \mathcal{B},\ \forall p \in \mathcal{P} \quad (5)$$

Constraints (4) ensures that each block is extracted at most once. Constraints (5) states that a block can be sent to only one destination.

Slope constraints

$$\sum_{d\in\mathcal{D}} x_{i,d,p} \leq \sum_{d\in\mathcal{D}} x_{j,d,p} \qquad \forall i \in \mathcal{B},\ \forall j \in \Gamma_i^-,\ \forall p \quad \in \mathcal{P} \quad (6)$$

A block i is available for extraction only if all of its direct predecessors Γ_i^- have already been extracted or are extracted in the same period.

Quantity constraints

Upper bound

$$\sum_{i\in\mathcal{B}} (q_{c_1,i,s} \cdot (x_{i,d,p} - x_{i,d,p-1})) - dev^{+}_{c_1,p,s} \ \leq target^{+}_{c_1,p}$$
$$\forall c_1 \in \mathcal{C}_1,\ \forall d \in \mathcal{D},\ \forall p \in \mathcal{P},\ \forall s \in \mathcal{S} \quad (7)$$

Lower bound

$$\sum_{i\in\mathcal{B}} (q_{c_1,i,s} \cdot (x_{i,d,p} - x_{i,d,p-1})) + dev^{-}_{c_1,p,s} \ \geq target^{-}_{c_1,p}$$
$$\forall c_1 \in \mathcal{C}_1,\ \forall d \in \mathcal{D},\ \forall p \in \mathcal{P},\ \forall s \in \mathcal{S} \quad (8)$$

Constraints (7) and (8) are soft constraints for the upper- and lower-bounds of the total quantities (mined or processed) in each period and in each scenario. The variables $dev^{\pm}_{c_1,p,s}$ are used as buffers to allow deviations but these deviations are penalized in the objective function.

Grade quality constraints

Upper bound

$$\sum_{i\in\mathcal{B}}(g_{c_2,i,s}\cdot t_{i,s}\cdot(x_{i,d,p}-x_{i,d,p-1}))-dev^{+}_{c_2,p,s} \leq target^{+}_{c_2,p}\cdot\sum_{i\in\mathcal{B}}(t_{i,s}\cdot(x_{i,d,p}-x_{i,d,p-1})) \quad \forall c_2\in\mathcal{C}_2, d=1,\ \forall p\in\mathcal{P},\forall s\in\mathcal{S} \quad (9)$$

Lower bound

$$\sum_{i\in\mathcal{B}}(g_{c_2,i,s}\cdot t_{i,s}\cdot(x_{i,d,p}-x_{i,d,p-1}))+dev^{-}_{c_2,p,s} \geq target^{-}_{c_2,p}\cdot\sum_{i\in\mathcal{B}}(t_{i,s}\cdot(x_{i,d,p}-x_{i,d,p-1})) \quad \forall c_2\in\mathcal{C}_2, d=1,\ \forall p\in\mathcal{P},\forall s\in\mathcal{S} \quad (10)$$

Similar to the capacity constraints, constraints (9) and (10) penalize excess and shortage of the average grade c_2 at each period and for each scenario.

Extraction smoothing constraints

$$\sum_{d\in\mathcal{D}}x_{i,d,p}\leq\sum_{d\in\mathcal{D}}x_{j,d,p} \qquad \forall i\in\mathcal{B}^{1/2},\ \forall j\in\mathcal{N}(i),\ \forall p\in\mathcal{P} \quad (11)$$

These operational constraints impose a continuous sequence of extraction in a way that the blocks that are directly adjacent to a block i must also be extracted in the same period.

Earliest period of extraction constraints

$$x_{i,d,p}=0 \qquad \forall i\in\mathcal{B},\ \forall d\in\mathcal{D}, \quad \forall p\in\left\{\bigcup_{c_1\in\mathcal{C}_1}\left(t\in\mathcal{P};\ \forall s\in\mathcal{S},\sum_{t'=1}^{t}target^{+}_{c_1,t'}-\Delta_{c_1,t'}\ \leq\sum_{j\in\Gamma_i^{-Tot}\cup\{i\}}q_{c_1,j,s}\right)\right\} \quad (12)$$

These constraints, equivalent to an earliest start of a job, are optional. They eliminate variables to make the model easier to solve. To reach a block i by period p, at least all of its full cone of predecessors Γ_i^{-Tot} must be extracted. This cone, in addition to block i, represents a certain tonnage or quantity that is compared to the sum of the targets from periods $\{1,\ldots,p\}$. In these cases, the corresponding variables $x_{i,d,p}$ can be set to 0, which forces block i to not be extracted in period p. Typically, one may take $\Delta_{c_1,t'}\cong\frac{1}{4}*target^{+}_{c_1,t'}$.

2.2.3 Partial relaxation

Partial relaxation is used to reduce the number of binary variables and accelerate the solution process. First, an initial feasible solution of the model is obtained by relaxing the binary variables associated with the waste blocks; this reduces the number of binary variables without affecting the integrality of the ore blocks (Leite and Dimitrakopoulos, 2014). The partial relaxation returns a fractional schedule, which is then used as an input for a heuristic algorithm to obtain a final result close to the initial formulation.

From the relaxed or partially relaxed solution, two sets of weights $\{w1_i,\ \forall i\in\mathcal{B}\}$ and $\{w2_{i,d},\ \forall i\in\mathcal{B},\ \forall d\in\mathcal{D}\}$, which are later used in the TopoSort algorithm.

$$E1_i = \sum_{p\in\mathcal{P}} p * \sum_{d\in\mathcal{D}} \left(x^*_{i,d,p} - x^*_{i,d,p-1}\right) + (P+1)\left(1 - \sum_{d\in\mathcal{D}} x^*_{i,d,\ P}\right) \qquad \forall i \in \mathcal{B} \tag{13}$$

$$w1_i = -E1_i \qquad \forall i \in \mathcal{B} \tag{14}$$

$$w2_{i,d} = \sum_{p=1}^{P} \left(x^*_{i,d,p} - x^*_{i,d,p-1}\right) \qquad \forall i \in \mathcal{B}, \forall d \in \mathcal{D} \tag{15}$$

$E1_i$ is defined as the expected value of the extraction period of block i. Given that the weight $w1_i = -E1_i$, a larger weight indicates that the optimizer wishes to extract the block sooner. The weight $w2_{i,d}$ represents the faction of block i sent to destination d. This is used to determine the most likely destination for a block. Both sets of weights are then given to a heuristic algorithm an input that allows it to be as close as possible to the relaxed solution while respecting the various constraints.

2.2.4 Heuristic method

The partial relaxation above provides a fractional solution. To generate the final binary solution, as needed for the SOPMPS model, the heuristic method by Rimélé (2016) is implemented. The method is an application of a topological sort algorithm (TSA), similar to Chicoisne et al. (2012), adapted to a stochastic formulation with several destinations. The main idea is to first order the blocks by their "expected period of extraction", which is obtained for each block as the sum of the percentage of extraction (extraction variable from the fractional solution) times the period of extraction. The TSA is then an iterative process that, at each iteration, will consider the subset of accessible blocks (blocks with no direct predecessors), and select from them the first in the ordered list. If from the fractional solution, most of this block was sent to the waste dump, then this block is fully mined in the current period and also sent to the waste dump in the binary solution. However, if the block was mainly sent to the mill in the fractional solution, two options are possible: if its tonnage in less than the remaining processing capacity, the block is fully processed in the current period; if it does not fit in the remaining capacity, the current period is incremented and the block is assigned to this new period. The intent of this method is to remain as close as possible to the fractional solution while providing a binary solution.

3 Case study: Application at an iron ore deposit

The previously outlined methodology is applied to an iron ore deposit in northern Quebec, Canada. This deposit consists of banded sedimentary rocks that are primarily composed of bands of iron oxides, magnetite and hematite within quartz (chert)-rich rock with variable amounts of silicate, carbonate and sulphide lithofacies. The deposit has seven iron–bearing layers and two overlying layers considered as waste material. The layers contain four strongly-correlated qualities of interest: head iron grade (FeH), the Davis Tube Weight Recovery (DTWR), the Davis Tube concentrate grade (FeC), and the Davis Tube concentrate silica grade (SiO_2). Two variables (grades) are considered to control the production process: the average DTWR grade and the average silica per period. Silica concentration in the input feed material represents the main pollutant for iron ore processing, and is crucial for maintaining the quality of the metal production. The production scheduling is done over a life-of-mine of 10 years and two destinations are considered: the "mill" for processing the ore and the "waste dump" for disposing the waste material.

3.1 Stochastic simulation of the iron ore deposit

3.1.1 Simulation of lithologies

The WAVESIM algorithm is used to generate the simulations of the seven iron-bearing and two waste lithologies. The training image, which serves as a pattern database for the simulation algorithm, has been created using a geological interpretation based on a set of wireframes provided by the mine. The wireframes

are discretized in a Cartesian grid of 70x100x26 blocks in the x-, y- and z-directions, respectively, with a cell size of 100x100x15 m^3. Therefore, total of 182,000 nodes are simulated. The simulations are validated in terms of histograms, variograms, and high-order statistics by comparing to the training image and the hard data (e.g. drillholes). High-order statistics are validated with high-order spatial cumulants (Dimitrakopoulos et al., 2010).

Figure 3 shows the results obtained from simulation of the mine's lithological boundaries. The training image (left) and two simulations randomly selected from the fifteen available (right). From the comparison of the sections of the TI and simulations, it seen that the simulations respect the same spatial layering as the TI, given that each lithology tends to appear in the same region. However, as expected, the simulated realizations are "patchy" and present more variable patterns when compared to the TI.

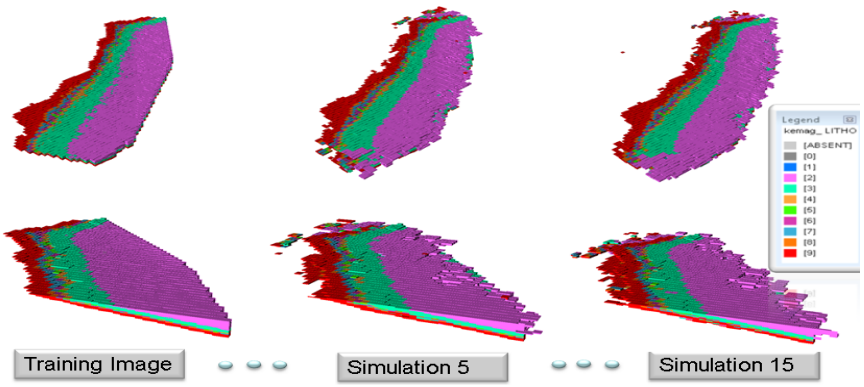

Figure 3: Cross sections (right Training Image, left simulations).

Figure 4 shows the reproduction of the histograms for the simulations, TI and hard drilling data (HD). The fifteen simulations reproduce the proportions of the lithologies of the deposit. The lithologies "3–LC" and "9–LRGC" have the highest proportions by volume. The proportions of the simulations for 3–LC are higher than the TI and HD proportions due to the fact that *WAVESIM* reproduces the simulation on a cubic 3D-grid. Thus, as lithology 3–LC is closer to the surface, it has more "empty space" at the edges of the grid to paste patterns belonging to this category. Some post-processing methodologies can be applied to constraint the simulation grid and avoid this. Regardless, the proportions for all other lithologies are very close to the hard data and training image proportions.

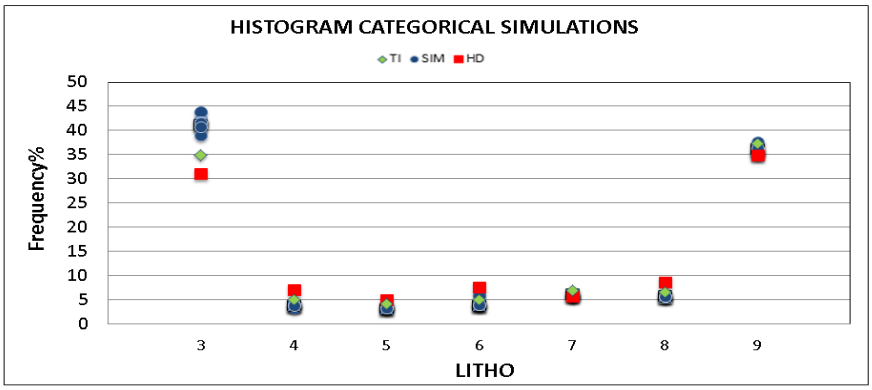

Figure 4: Histogram of categorical simulations compared to hard data and training image.

Indicator variograms are used to validate the spatial continuity for each of the lithologies. Figure 5 and 6 show the indicator variograms for lithology 3-LC and 9-LRGC, respectively, in two directions for the 15 simulations along with the hard data and training image. The results suggest a reasonable reproduction of the variogram for the simulations compared to the TI and HD. Figures 7 and 8 show the cross-variograms

for the two key ore layers in the North-South and East-West directions, respectively. Results show that the simulations are following the same behavior and relation as the HD and TI.

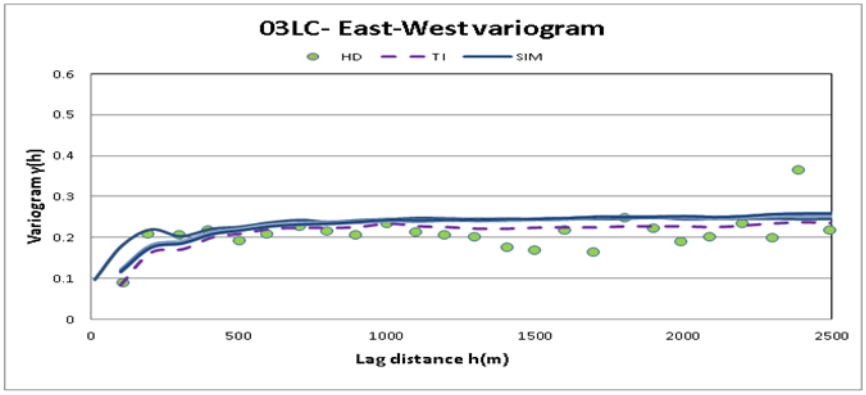

Figure 5: Variogram of categorical simulation for lithology 3-LC, compared to HD and TI.

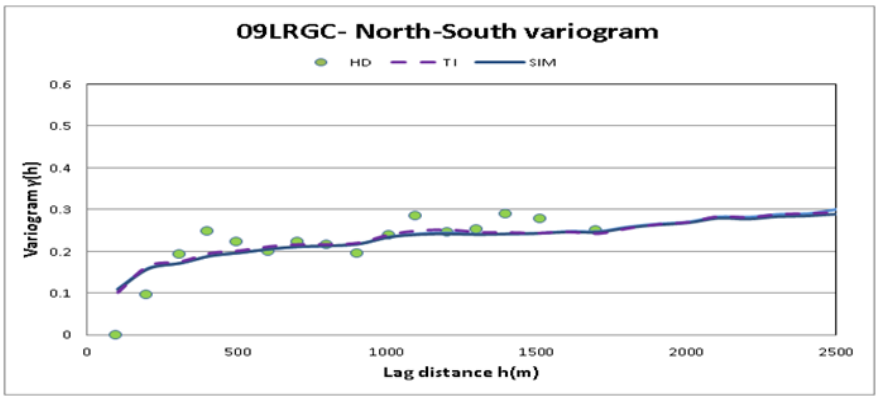

Figure 6: Variogram of categorical simulation for lithology 9LRGC, compared to HD and TI.

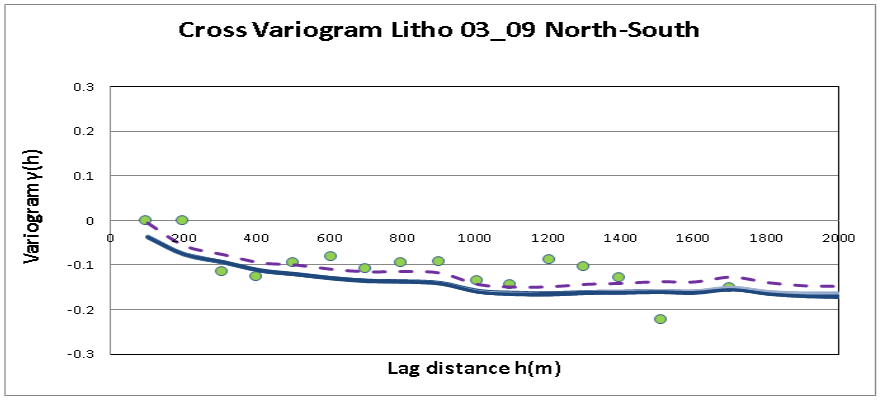

Figure 7: Cross-variograms of the ore lithologies in the North-South directions.

Given that *WAVESIM* is a pattern-based simulation method, the high-order relations should be reproduced by the simulations. Therefore, validations are also performed for the high-order statistics using cumulant maps. To generate the cumulant map, an "L-Shape" template is used to calculate the 3rd-order cumulant along the vectors in the (1, 0, 0) and (0, 1, 0) directions. Figure 8 shows the cumulant map calculated for the lithology "3–LC" for the TI and two randomly selected simulations. It is noted that the cumulant maps of the simulations show a similar pattern as the TI for the first 2-km in the North direction

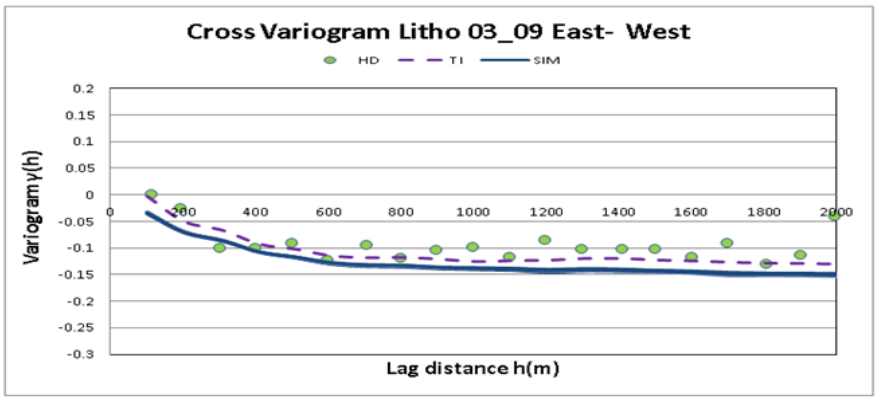

Figure 8: Cross-variograms of the ore lithologies in the East-West directions.

and the first 500-m along the East direction. The lithologies have a strong correlation in this area, which is represented by the high values in the cumulant map (i.e., the red area in Figure 9). Given that the orebody has a high North-South strike length, the high cumulant values show more continuity in North-South direction. It can be also seen that the extension of the orebody in the North-South direction is well reproduced by the simulations. However, after 500m, the North direction shows very little spatial continuity. This is related to the sparse density of the drillholes.

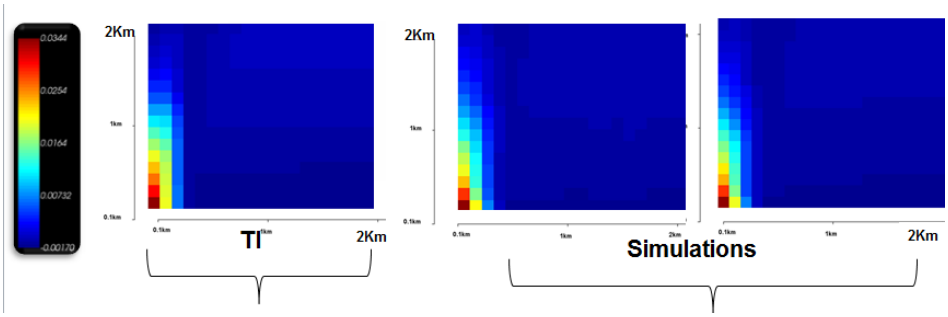

Figure 9: Third-order cumulant map for Training Image (left) and two simulations (right).

WAVESIM retrieves statistics from the TI and the hard data (drillholes), however, the distance between drillholes for the deposit is large, making it is difficult to obtain a cumulant map for the hard data. Results for validation of the lithological boundaries simulation in terms of low-order statistics (histogram and variograms) and high-order statistics (cumulant maps), indicates that, in general, all fifteen simulations well-reproduce the spatial features of the drillholes information and training image.

3.1.2 Simulation of continuous variables (grades)

The grades of the attributes of interest, head iron grade (FeH), Davis Tube Weight Recovery (DTWR), Davis Tube concentrate grade (FeC), and the Davis Tube concentrate silica grade (SiO_2), are then simulated at the block-support scale using *DBMAFSIM* within the lithological boundaries generated using the *WAVESIM* algorithm. To validate the simulations generated using *DBMAFSIM*, the simulated point-scale values from the data space are used.

Figure 10 shows the plan view of the four simulated elements within simulated boundaries of the lithologies, highlighting that, despite presenting different boundaries because they are simulated inside different categorical orebody simulations, the simulations of grade attributes tend to reproduce the same spatial pattern of the drillholes information because they coincide with high-grade and low-grade areas between the simulations. Figure 11 shows the histograms of the simulated grades within the 5-GC lithology. Although 5-GC is not considered significant because of its' low iron content, this lithology is one of the thinnest layers, therefore, this lithology was chosen to represent the results of this application.

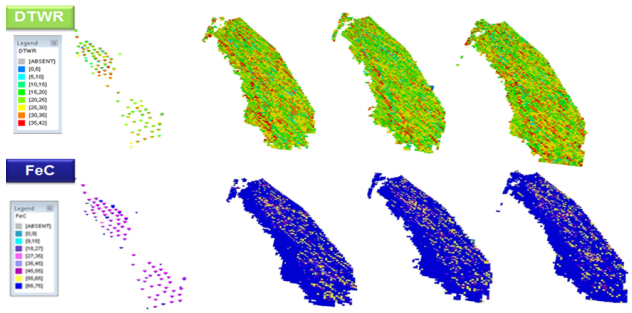

Figure 10: Plan view of hard data (drillholes) and some simulations for two grade simulated.

Figure 12 shows variograms and cross-variograms for the hard data and the simulations on the point-support scale within the 9-LRGC lithology. Overall, the simulations reproduce the spatial features of the hard data. The simulation variograms are reasonably consistent with the hard data for a range of 2-km.

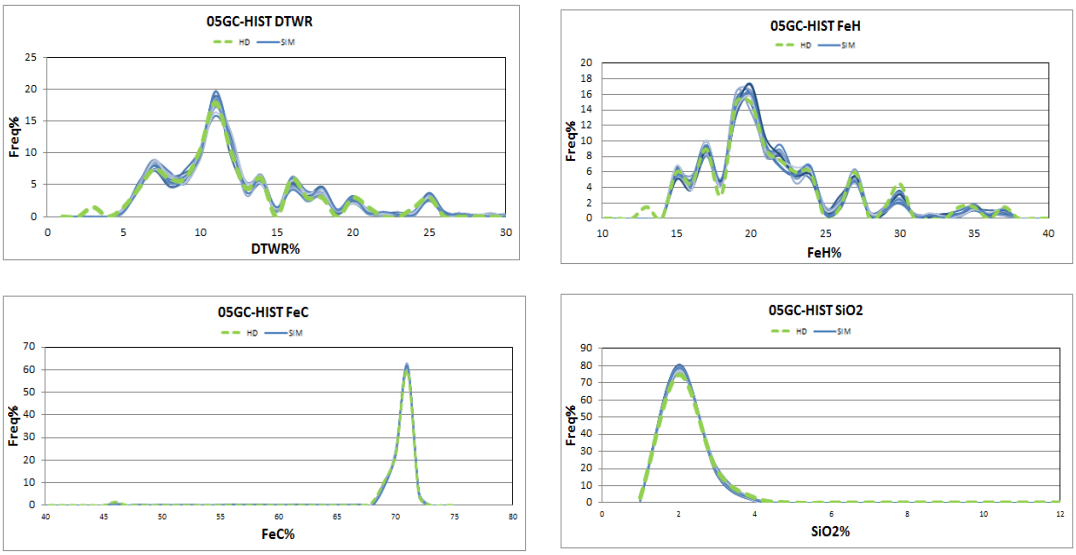

Figure 11: DTWR and FeC and FeH and SiO_2 histogram for a single lithology 5-GC.

3.2 Stochastic life-of-mine production schedule

A 10-year mine production schedule is generated using the previously defined stochastic optimization model with a yearly production target of 10-Mt of iron ore concentrate. The metallurgical plant is designed and optimized for a concentrator with an average input of a DTWR of 27%. The production of fine iron concentrate is generated through beneficiation and can be sold as a final product. The performance of the metallurgical plant might be affected by the silica content, which should lie between 2.3% and 2.9%.

The results of the stochastic mine production scheduling using 15 simulations of the deposit are shown in Figures 13 to 18. Note that the presented results represent the fully binary solution of the relaxed model obtained using the Topological Sort Algorithm. Figure 13 shows the extraction sequence and block destinations. The areas describe a practical mining sequence that considers the layered strata of the deposit and the size of the blocks. Figure 13 also shows that the first period is where the waste lithologies (layers) are extracted, which is due to the fact the waste lithologies are mostly overlying the ore material. It is noted that some artifacts, in the form of isolated mining blocks, exist in some periods; this could be improved using better pre-processing algorithms, however, it has not been considered in the current work.

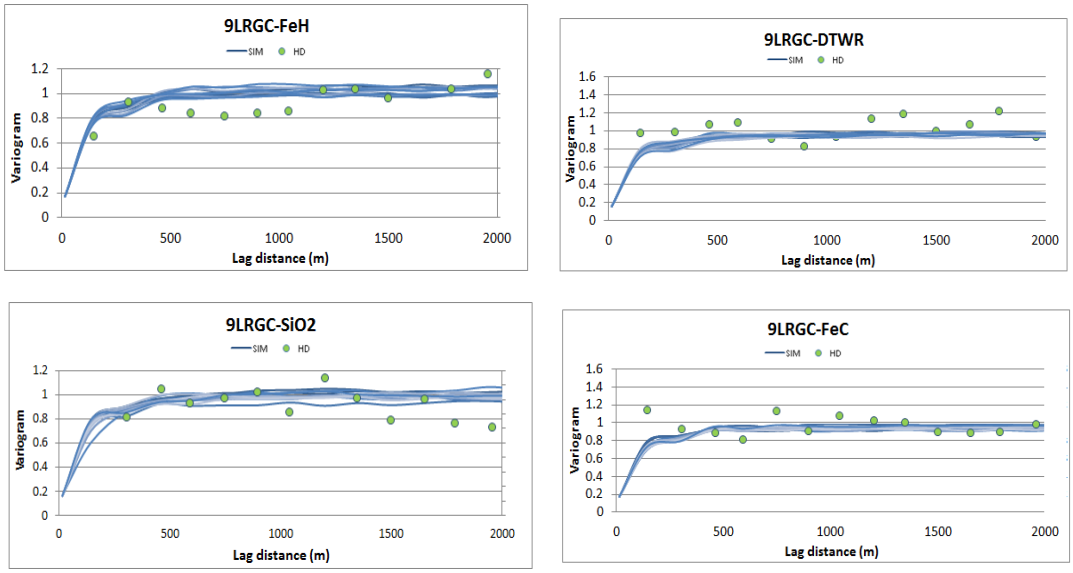

Figure 12: Point-variograms of grades within the 9-LRGC lithology.

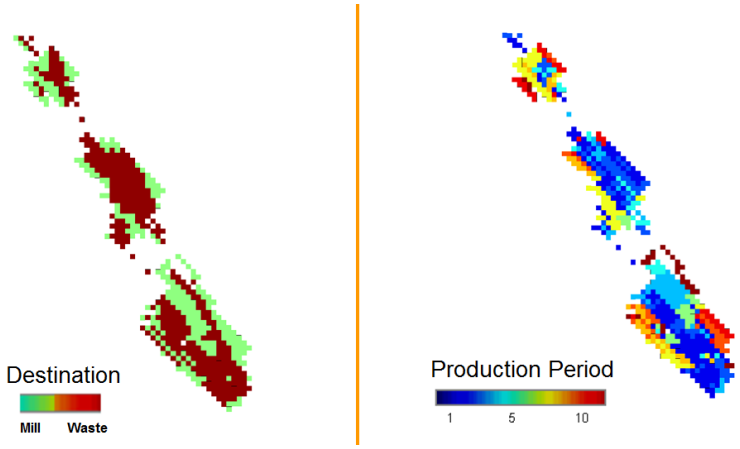

Figure 13: Plan view of the block destinations (left) and the extraction sequence (right).

The solution of the relaxed model is considered to be the upper-bound for the binary solution of the SOPMPS model. The tonnage and qualities for each period are evaluated for each simulation to analyze the variability. Figure 14 shows that the schedule is unable to fulfill the target of 10 million tonnes per year. The run of mine (ROM) material sent to the mill, which is not constrained, is shown in Figure 15. It can be seen that the differences between the simulations are not significant, which is important when selecting the mining equipment (shovels and trucks). Achieving the targeted concentrate tonnage is usually one of the main goals of production scheduling. Nevertheless, from Figure 16, a steady behavior of DTWR production can be seen, varying within the expected ranges and averagely around 27%, which is desired for the concentrator. It is important to note that the annual fluctuations of concentrate production are balanced by the DTWR production. For instance, a year with less concentrate production has a greater average weight recovery, which implies that less ore must be mined to produce the same tonnage of concentrate. On the other hand, from Figure 17, it can be seen that silica production deviates from production targets in the last periods. The average amount of silica must be kept beneath a certain level when pellet production is desired, given that silica is considered as an impurity and affects the selling price. Given that this project is in the feasibility stage, the project is being evaluated in terms of its practical and financial viability. Thus, these results are useful for the company and provide valuable information such as planed concentrate iron production of 10 Million tonnes per year might not be achievable.

Figure 18 shows the discounted cash flows (DCF) for all the scenarios and their average. It is observed that the scenarios do not present significant deviations from the average, except for period six and seven, where the DCF fluctuates in the order of 4%. This is caused by a higher SiO_2 % this period (see Figure 16), thus the penalties applied to the silica deviations affects the revenue. This result might be considered acceptable because the risk is deffered to later periods with the applied risk discounting factor and is same as the economic discount factor.

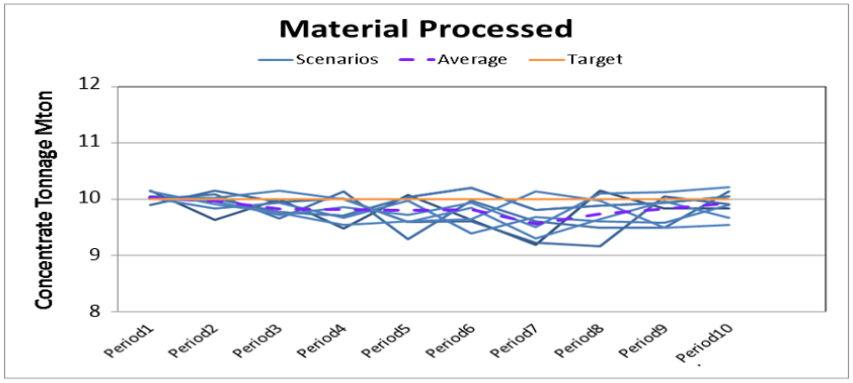

Figure 14: Yearly iron ore concentrate tonnes.

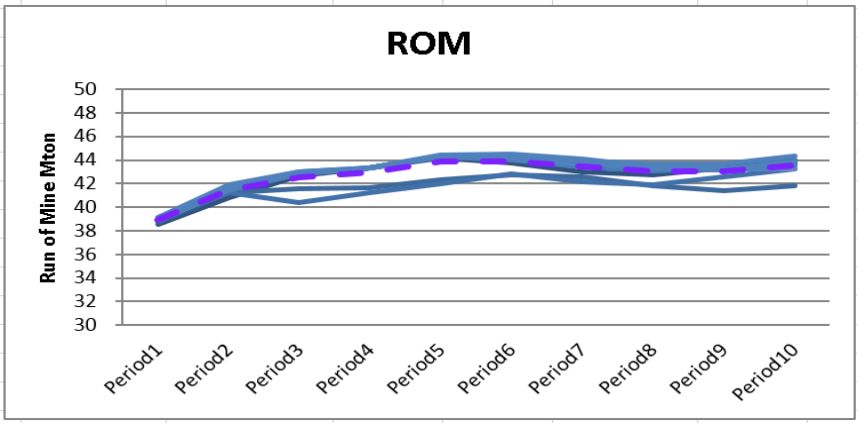

Figure 15: Yearly ROM.

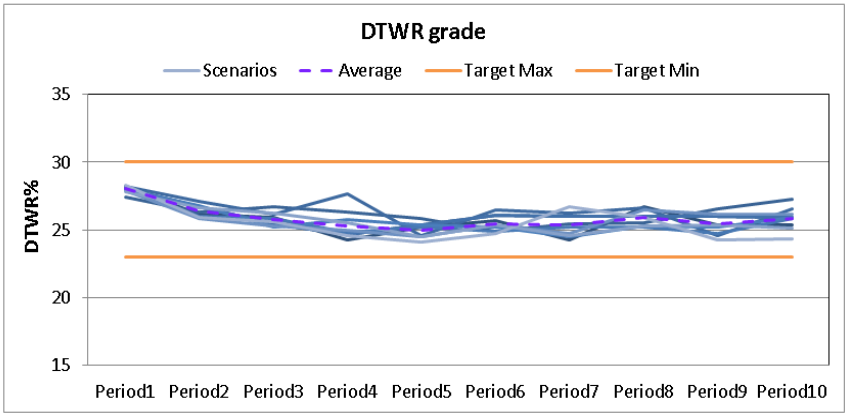

Figure 16: Yearly DTWR% production.

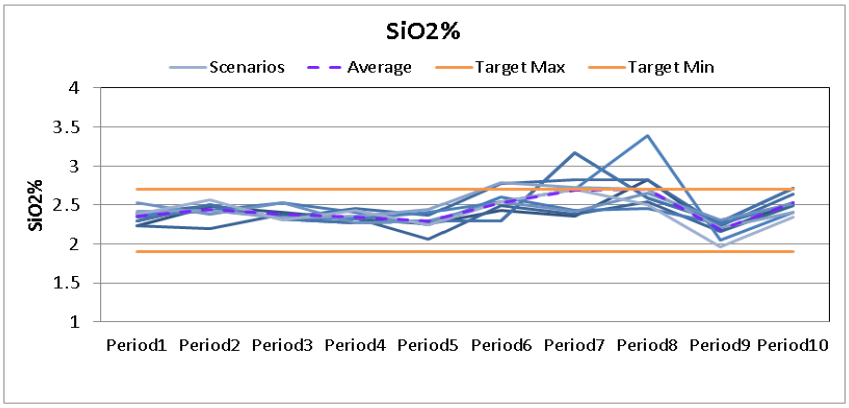

Figure 17: Yearly silica production.

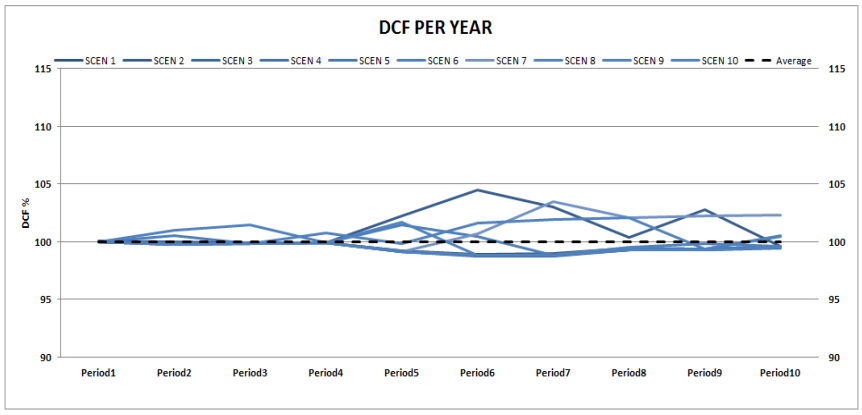

Figure 18: Yearly discounted cash flow (DCF %).

4 Conclusions

This paper presents the application of a stochastic mine planning framework to an iron ore mine located in northern Quebec, Canada. The case study includes the two steps of the method used, firstly, the generation of a set of equally probable realizations of the deposit and, secondly, the optimization of long-term mine production schedule that manages the inherent geological risk. To quantify the volumetric uncertainty of the deposit, the pattern-based *WAVESIM* algorithm is used to model the seven iron–bearing layers and two overlying waste layers. The *DBMAFSIM* is then used to jointly-simulate the head iron (FeH), the Davis Tube weight recovery (DTWR), Davis Tube concentrate iron (FeC) and silica grade. The generated set of simulations are validated in terms of lower-order statistics (variograms and histograms) and third-order cumulant maps. The statistics of the realizations are compared to both the training image and the drillholes samples statistics, which indicate that reproduction of the critical features of *WAVESIM* is driven by the training image. It is, therefore, critical that the training image is be representative of the deposit in order to obtain valid simulations.

The validated simulations of the iron deposit are used as input for the stochastic optimization of the production schedule using a methodology that seeks to obtain efficient solutions to the production scheduling problem that maximizes the expected value of the discounted cash flows and simultaneously manages geological risk. Geological risk management for the outlined production schedule problem is incorporated by strictly reducing risk in the earlier years i.e., minimizing the risk of deviation from concentrate tonnage targets and produced silica target. It is shown that the production tonnages and silica grade qualities can vary significantly, particularly in the final years of the life of mine. This result is not surprizing because the project is currently in the feasibility stage. The SIP framework applied here also allows for easily balancing

multiple goals simultaneously, which is otherwise a challenging task. Although a computational time comparison and optimality analysis of the solution was out of scope of this exercise, from the application of the SOPMPS combined with an acceleration method the results were obtained in the order of minutes, yielding robust results in terms of accounting for the inherent geological uncertainty.

References

Albor Consuegra, F., and Dimitrakopoulos, R. (2010) An algorithmic approach to pushback design based on stochastic programming: Method, application and comparisons. IMM Trans, Mining Technology 119(2):68–83

Arpat, G., and Caers, J. (2007) Conditional simulation with patterns. Mathematical Geology, 39(2): 177–203.

Benndorf, J. (2005) Efficient sequential simulation methods with implications to long-term production scheduling. MPhil Thesis, Dept. of Mining and Materials Processing Engineering, The University of Queensland, Brisbane, Qld, Australia.

Benndorf, J., and R. Dimitrakopoulos (2013) Stochastic long-term production scheduling of iron ore deposits: integrating joint multi-element geological uncertainty. Journal of Mining Science 49(1): 68–81.

Birge, J. R., and Louveaux, F. (2011) Introduction to stochastic programming. Springer Series in Operations Research, 2nd Edition, Berlin.

Boucher, A., and Dimitrakopoulos, R. (2009) Block simulation of multiple correlated variables. Mathematical Geosciences, 41(2):215–237.

Boucher, A., and Dimitrakopoulos, R. (2012) Multivariate block-support simulation of the Yandi iron ore deposit, Western Australia. Mathematical Geosciences, 44(4): 449–468.

Chatterjee, S., Dimitrakopoulos, R., and Mustapha, H. (2012) Dimensional reduction of pattern-based simulation using wavelet analysis. Mathematical Geosciences, 44(3): 343–374.

Chicoisne, R., Espinoza, D., Goycoolea, M., Moreno, E., and Rubio, E. (2012) A new algorithm for the open-pit mine production scheduling problem. Operations Research, 60(3): 517–528.

Davis, M. D. (1987) Production of conditional simulations via the LU triangular decomposition of the covariance matrix. Mathematical Geology, 19(2): 91–98.

Desbarats, A., and Dimitrakopoulos, R. (2000) Geostatistical simulation of regionalized pore-size distributions using min/max autocorrelation factors. Mathematical Geology, 32(8): 919–942.

Dimitrakopoulos, R., and Jewbali, A. (2013) Joint stochastic optimization of short- and long- term mine production planning: Method and application in a large operating gold mine. Mining Technology, 122(2):110–123

Dimitrakopoulos, R., and Ramazan, S. (2004) Uncertainty based production scheduling in open pit mining. SME Transactions, 316:106–112

Dimitrakopoulos, R., Mustapha, H., and Gloaguen, E. (2010) High-order statistics of spatial random fields: exploring spatial cumulants for modelling complex, non-Gaussian and non-linear phenomena. Mathematical Geosciences 42(1): 65–99.

Ding, C., and He, X. (2004) K-means clustering via principal component analysis. Proceedings of the twenty-first international conference on Machine learning. ACM.

Godoy, M. (2002) The effective management of geological risk in long-term production scheduling of open pit mines. PhD thesis, Dept. of Mining and Materials Processing Engineering, University of Queensland, Brisbane, Australia.

Goodfellow, R., Albor, F., Dimitrakopoulos, R., and Lloyd, T. (2012) Quantifying multi-element and volumetric uncertainty Coleman McCreedy deposit, Ontario, Canada. Computers and Geosciences, 42(1): 71–78.

Goodfellow, R., and Dimitrakopoulos, R. (2016) Global Asset Optimization of Open Pit Mining Complexes under Uncertainty. Applied Soft Computing, 40(1): 292–330.

Goovaerts, P. (1997) Geostatistics for Natural Resources Evaluation (Applied Geostatistics Series). Oxford University Press, Oxford.

Lamghari, A., and Dimitrakopoulos, R. (2012) A diversified Tabu search approach for the open-pit mine production scheduling problem with metal uncertainty. European Journal of Operational Research, 222(3): 642–652.

Lamghari, A., Dimitrakopoulos, R., and Ferland, J. (2013) A variable neighborhood descent algorithm for the open-pit mine production scheduling problem with metal uncertainty. Journal of Operational Research Society, (1):1–28.

Leite, A. (2007) Stochastic optimization approaches to open pit mine planning: Applications for and the value of stochastic approaches. MEng Thesis, Department of Mining and Materials Engineering, McGill University, Montreal, Quebec, Canada

Leite, A., and Dimitrakopoulos, R. (2014) Stochastic optimization of mine production scheduling with uncertain ore/metal/waste supply. International Journal of Mining Science and Technology 24(1):755–762

Lopes, J., Rosas, C., Fernandez, J., and Vanesa, G. (2011) Risk quantification in grade-tonnage curves, and resource categorization in a lateritic nickel deposit using geologically constrained Joint conditional simulation. Journal of Mining Science and Technology, (2): 166–176.

Montiel, L., Dimitrakopoulos, R., and Kawahata, K. (2016) Globally optimising open-pit and underground mining operations under geological uncertainty. Mining Technology, 125(1): 2–14

Ramazan, S., and Dimitrakopoulos, R. (2004) Traditional and new MIP models for production scheduling with in-situ grade variability. International Journal of Surface Mining, Reclamation and Environment, 18(2):85–98.

Ramazan, S., and Dimitrakopoulos, R. (2005) Stochastic Integer Programming for Optimizing of long term production scheduling for open pit mines with a new integer programming formulation. In, Orebody Modelling and Strategic Mine Planning: Uncertainty and Risk Management Models, AusIMM, Spectrum Series 14(1):359–366.

Ramazan, S., and Dimitrakopoulos, R. (2013) Production scheduling with uncertain supply: A new solution to the open pit mining problem. Optimization and Engineering, 14(2): 361–380.

Rimélé, A. (2016) Méthode heuristique d'optimization stochastique de la planification minire et positionnement des résidus miniers dans la fosse. MSc Thesis, Universite de Montreal département de mathématiques et de génie industriel cole Polytechnique de Montréal. Montreal, Quebec, Canada.

Spleit, M. (2014) Production schedule optimization-meeting targets by geological risk while addressing environmental and Equipment concerns. Orebody modelling and strategic mine planning symposium, (1): 397–403

Strebelle, S. (2002) Conditional simulation of complex geological structures using multiple-point geostatistics. Mathematical Geology, 34(1): 1–22.

Zhang, T., Switzer, P., and Journel, A. (2006) Filter-based classification of training image patterns for spatial simulation. Mathematical Geology, 38(1): 63–80.